

Article

Smooth-Switching Gain Based Adaptive Neural Network Control of n-Joint Manipulator with Multiple Constraints

Qing Yang ^{1,2}, Haisheng Yu ^{1,2,*}, Xiangxiang Meng ^{1,2}, Wenqian Yu ³ and Huan Yang ⁴

¹ College of Automation, Qingdao University, Qingdao 266071, China; 2020020573@qdu.edu.cn (Q.Y.); 2018020450@qdu.edu.cn (X.M.)

² Shandong Province Key Laboratory of Industrial Control Technology, Qingdao University, Qingdao 266071, China

³ State Grid Dongping Power Supply Company, State Grid, Taian 271000, China; yuwenqiandp@163.com

⁴ School of Mechanical and Automotive Engineering, Qingdao University of Technology, Qingdao 271000, China; 13675327120@139.com

* Correspondence: yhsh_qd@qdu.edu.cn

Abstract: Modeling errors, external loads and output constraints will affect the tracking control of the n-joint manipulator driven by the permanent magnet synchronous motor. To solve the above problems, the smooth-switching for backstepping gain control strategy based on the Barrier Lyapunov Function and adaptive neural network (BLF-ANBG) is proposed. First, the adaptive neural network method is established to approximate modeling errors, unknown loads and unenforced inputs. Then, the gain functions based on the error and error rate of change are designed, respectively. The two gain functions can respectively provide faster response speed and better tracking stability. The smooth-switching for backstepping gain strategy based on the Barrier Lyapunov Function is proposed to combine the advantages of both gain functions. According to the above strategy, the BLF-ANBG strategy is proposed, which not only solves the influence of multiple constraints, unknown loads and modeling errors, but also enables the manipulator system to have better dynamic and steady-state performances at the same time. Finally, the proposed controller is applied to a 2-DOF manipulator and compared with other commonly used methods. The simulation results show that the BLF-ANBG strategy has good tracking performance under multiple constraints and model errors.

Keywords: manipulator; multiple constraints; adaptive neural network; smooth-switching for gain; Barrier Lyapunov Function



Citation: Yang, Q.; Yu, H.; Meng, X.; Yu, W.; Yang, H. Smooth-Switching Gain Based Adaptive Neural Network Control of n-Joint Manipulator with Multiple Constraints. *Actuators* **2022**, *11*, 127. <https://doi.org/10.3390/act11050127>

Academic Editors: Marco Carricato and Edoardo Ida

Received: 1 February 2022

Accepted: 25 April 2022

Published: 29 April 2022

Publisher's Note: MDPI stays neutral with regard to jurisdictional claims in published maps and institutional affiliations.



Copyright: © 2022 by the authors. Licensee MDPI, Basel, Switzerland. This article is an open access article distributed under the terms and conditions of the Creative Commons Attribution (CC BY) license (<https://creativecommons.org/licenses/by/4.0/>).

1. Introduction

The manipulator has been widely used in various scenarios such as medical treatment, automobile production and metal processing due to its strong safety, high precision and high efficiency [1–3]. The permanent magnet synchronous motor (PMSM) has the characteristics of small size, low loss and large starting torque [4,5], which is often used as the drive motor for the servo control of the manipulator [6,7]. The manipulator system driven by PMSM is a multi-variable, nonlinear and strongly coupled system. Therefore, as the production requirements increase, the rapidity, accuracy and stability of manipulator tracking have always been a research hotspot.

For manipulator tracking control, many scholars have proposed different control strategies. Traditional control strategies such as proportional integral derivative (PID) control, feedback linearization control, sliding mode control (SMC), adaptive control and backstepping control are commonly used. Intelligent control methods such as fuzzy control and neural network control are also widely used. Shojaei, Pradhan, and Kim respectively used self-tuning PID control, second-order PID control and PD control to effectively improve the steady-state tracking performance of the manipulator [8–10]. Feng, Yeh, and Huang respectively designed non-singular fast terminal SMC strategy [11], output

feedback SMC strategy [12] and adaptive SMC strategy [13]. Each method optimizes the traditional SMC strategy, however, the chattering phenomenon still exists. Gabriele and Meng adopted the feedback linearization strategy [14,15], but this strategy requires an accurate mathematical model. In literature [16–18], adaptive control was designed to effectively estimate the uncertainty of the system. Kanellakopoulos proposed a recursion-based backstepping control [19], which was then widely used. Cheng and Farrell applied backstepping strategy to the control of the manipulator [20,21]. Chang, Yang and Song designed fuzzy backstepping, fuzzy adaptive and fuzzy command filter controllers to improve the stability of position tracking [22–24]. The neural network control has strong approximation ability, so it is used by many scholars to approximate the modeling errors and nonlinear terms [25–28].

The above methods have improved the dynamic and steady-state performances of manipulator tracking, respectively, however, it is difficult to guarantee better dynamic and steady-state performance at the same time. In addition, most of the existing strategies only consider the manipulator system and ignore the drive motor system, along with failing to consider the effects of multiple constraints, unknown loads and modeling errors at the same time. These problems often affect the safe and smooth operation of the manipulator in engineering practice. Many scholars have devised different solutions to these problems. Singh proposed the modeling concept of fractional calculus [29,30], and systematically described the fractional order model of the manipulator in the book [31]. The fractional order dynamic model can describe the system model more accurately. Meng and Liu adopted the coordination strategy of two controllers, combining the advantages of the two controllers to improve the dynamic and steady-state characteristics at the same time, but the use of two different controllers will increase the complexity of the control system [32,33]. Other studies [34–36] used the Barrier Lyapunov Function (BLF) to satisfy the output constraint problem. Sung and Cheng proposed a neural network strategy to approximate the model uncertainty [37,38]. Yang et al. designed a variable-gain backstepping strategy to improve the rapidity and stability of the controller [39–42].

In this paper, the smooth-switching for backstepping gain control strategy based on BLF and adaptive neural network (BLF-ANBG) is designed. Combined with the manipulator and the drive motor, the overall model of the manipulator control system is obtained. The adaptive radial basis function (RBF) neural networks are designed to approximate the modeling errors, unknown loads and unenforced inputs of the system. The gain function based on the error and the change rate of error is designed, and the Gaussian function is used as the switching function to design the method of smooth-switching for backstepping gain, which combines the advantages of the two gain functions. When the error is large, the gain function based on the error plays a major role, and the error is proportional to the gain, which shortens the rise time of the system. On the contrary, when the error is small, the gain function based on the change rate of error plays a major role, and the change rate of error is inversely proportional to the gain, which improves the stability of the steady-state of the system. The smooth-switching for backstepping gain controller is designed based on BLF (BLF-GSS) to realize the normal operation of the system under asymmetric or symmetric time-varying output limited. The BLF-ANBG strategy is proposed by combining the adaptive neural network strategy and the BLF-GSS strategy.

The main contents of this article are organized as follows. In Section 2, the overall model of the manipulator control system is provided by combining the manipulator system and the driven motor system. In Section 3, the BLF-ANBG controller based on an adaptive neural network and BLF-GSS is designed. In Section 4, the stability of the control strategy is proved by using the Lyapunov function [43]. In Section 5, the controller is applied to the 2-DOF manipulator, and the feasibility of the controller is verified by a simulation example. Some conclusions are summarized in Section 6.

2. The Overall System Model of n-Joint Manipulator Driven by PMSM

2.1. The Model of n-Joint Manipulator System

The system model of the n-joint manipulator considering the modeling error and unknown load is

$$(M(q) + \Delta M(q))\ddot{q} + (C(q, \dot{q}) + \Delta C(q, \dot{q}))\dot{q} + (G(q) + \Delta G(q)) = \tau_r - \tau_L - \tau_f - \Delta E \quad (1)$$

$$\tau_L = J^T F, \quad \tau_f = R_f \dot{q} + F_c \text{sgn}(\dot{q}) \quad (2)$$

where $q = [q_1, \dots, q_n]^T$ represents the position of each joint. $M(q)$ and $C(q, \dot{q}) \in R^{n \times n}$ are the positive-definite inertia matrix and Coriolis force matrix of the nominal model, respectively. $G(q) \in R^n$ is the system gravity vector of the nominal model. $\tau_r, \tau_L \in R^n$ and τ_f are respectively expressed as the output torque, load torque and friction torque of the manipulator system. $\Delta M(q), \Delta C(q, \dot{q})$ and $\Delta G(q)$ are the modeling error. J and F are the Jacobian matrix and load force of the manipulator, respectively. R_f and F_c are the diagonal viscous friction and Coulomb friction matrix. ΔE is the interference signal caused by position measurement error and velocity measurement noise.

2.2. The Model of Drive Motor System

The mathematical model of PMSM with modeling errors in the $d - q$ rotating coordinate system is described by

$$L_q \frac{di_q}{dt} = -n_p \Phi \omega - n_p B L_d i_d - R_s i_q + u_q \quad (3)$$

$$L_d \frac{di_d}{dt} = -R_s i_d + n_p B L_q i_q + u_d \quad (4)$$

$$(J_m + \Delta J_m) \frac{d\omega}{dt} = \tau - \tau_{mL} - R_m \omega \quad (5)$$

$$\frac{d\theta}{dt} = \omega \quad (6)$$

$$\tau = n_p [(L_d - L_q) i_d i_q + \Phi i_q] \quad (7)$$

where $\theta, \omega \in R^n$ indicate the rotation angle and speed of the PMSM. L_d, L_q is the diagonal square matrix of $d - q$ axis inductance. $B = \text{diag}\{\omega_1, \dots, \omega_n\}$, ω_i represents the i th component of the speed. i_d, i_q and u_d, u_q denote the $d - q$ axis stator current and voltage vector. n_p, Φ and $R_m \in R^{n \times n}$ are pole logarithm, magnetic flux and friction matrix of PMSM, respectively. $J_m \in R^{n \times n}$ denote the diagonal inertia matrix of PMSM. $\tau, \tau_{mL} \in R^n$ are the vector of electromagnetic torque and motor load torque, respectively. ΔJ_m denote the modeling error of PMSM.

Assumption 1. The input current of PMSM is strictly three-phase symmetrical.

Assumption 2. The core saturation of PMSM can be ignored.

Property 1. The manipulator system and the drive system are connected by the transmission with the reduction ratio of $\mu > 0$, that is $q = \mu\theta$ and $\tau_r = \mu^{-1}\tau_{mL}$.

2.3. The Overall Model of the Manipulator Driven by PMSM

According to (1)–(7), combined with the model of the manipulator system and the PMSM system, the dynamic model of the manipulator driven by PMSM with unknown load and modeling errors can be expressed as

$$\bar{M}(q)\ddot{q} + \bar{C}(q, \dot{q})\dot{q} + \bar{G}(q) = \tau - \mu(\tau_f + \tau_L + \Delta E) - \mu(\Delta M(q)\ddot{q} + \Delta C(q, \dot{q})\dot{q} + \Delta G(q)) - \mu^{-1}\Delta J_m \ddot{q} \quad (8)$$

where $\bar{M}(q) = \mu M(q) + \mu^{-1} J_m$, $\bar{C}(q, \dot{q}) = \mu C(q, \dot{q}) + \mu^{-1} R_m$, $\bar{G}(q) = \mu G(q)$

Considering the input saturation of the drive motor in the project, the actual input of PMSM electromagnetic torque $\tau_s(t) = [\tau_{s1}(t), \dots, \tau_{sn}(t)]^T$ is defined as

$$\tau_{si}(t) = \begin{cases} \tau_{i \max}, & \tau_i(t) \geq \tau_{i \max} \\ \tau_i(t), & \tau_{i \min} < \tau_i(t) < \tau_{i \max} \\ \tau_{i \min}, & \tau_i(t) \leq \tau_{i \min} \end{cases} \quad (9)$$

where the subscript i denotes the i th element of the electromagnetic torque vector. $\tau_{i \max}$, $\tau_{i \min}$ are the upper and lower limit values of the electromagnetic torque input to the drive motor, respectively. The part of the control signal that cannot be executed by PMSM can be expressed as

$$\tau_{ni}(t) = \tau_i(t) - \tau_{si}(t) = \begin{cases} \tau_i(t) - \tau_{i \max} & \tau_i(t) \geq \tau_{i \max} \\ 0 & \tau_{i \min} < \tau_i(t) < \tau_{i \max} \\ \tau_i(t) - \tau_{i \min} & \tau_i(t) \leq \tau_{i \min} \end{cases} \quad (10)$$

Substituting (4) and (5), Equation (3) is rewritten as

$$\bar{M}(q)\ddot{q} + \bar{C}(q, \dot{q})\dot{q} + \bar{G}(q) = \tau_s - \mu\tau_f + f(\mu, \tau_n, \tau_L, q, \dot{q}, \ddot{q}) \quad (11)$$

where $f(\mu, \tau_n, \tau_L, q, \dot{q}, \ddot{q}) = \tau_n - \mu(\tau_L + \Delta E) - \mu(\Delta M(q)\ddot{q} + \Delta C(q, \dot{q})\dot{q} + \Delta G(q)) - \mu^{-1}\Delta J_m\ddot{q}$, represents unknown modeling error, load and unexecuted input. For the convenience of the following application we use f instead of $f(\mu, \tau_n, \tau_L, q, \dot{q}, \ddot{q})$. Define the state vector as $x_1 = q, x_2 = \dot{q}$. The state equation of the manipulator system can be described as

$$\dot{x}_1 = x_2 \quad (12)$$

$$\dot{x}_2 = \bar{M}^{-1}(x_1)[- \bar{C}(x_1, x_2)x_2 - \bar{G}(x_1) + f + \tau_s - \mu\tau_f] \quad (13)$$

$$y = x_1 \quad (14)$$

In the actual servo tracking of the robot arm, it is necessary to ensure that the output of each joint is bounded and can normally track the desired position signal.

Assumption 3. *There exist time-varying output upper and lower bounds $y_{i \max}(t)$ and $y_{i \min}(t)$ ($i = 1, 2, \dots, n$), such that $y_{i \min}(t) \leq y_i(t) \leq y_{i \max}(t), \forall t > 0$.*

Assumption 4. *There are functions $y_{di \min}(t)$ and $y_{di \max}(t)$ that satisfy the inequality $y_{i \min}(t) \leq y_{di \min}(t)$ and $y_{di \max}(t) \leq y_{i \max}(t), \forall t > 0$, so that the desired position satisfies $y_{di \min}(t) \leq y_{di}(t) \leq y_{di \max}(t)$.*

Lemma 1 ([34]). *For any $|\zeta| < 1$, the inequality $\log \frac{1}{1-\zeta^2} < \frac{\zeta^2}{1-\zeta^2}$ is satisfied.*

3. Design of Controller

In this section, the structure and approximation process of the adaptive RBF neural network are described. Then, the smooth-switching for backstepping gain method is designed. Finally, the BLF-ANBG controller is designed.

3.1. Design of Adaptive Neural Network Approximation

To estimate modeling error, external load torque and unexecuted input, an adaptive RBF neural network strategy composed of an input layer, middle layer and output layer is designed. The structure of the adaptive RBF neural network is shown in Figure 1.

The middle layer is composed of five neurons, the output of each neuron is

$$h_k = \exp\left(-\frac{\|z - c_k\|^2}{b_k^2}\right) \quad (k = 1, \dots, 5) \quad (15)$$

where $z = [e_1, \dot{e}_1]^T$ is the input vector. c_k, b_k represent the center point vector and width of the k th neuron, respectively. The output of the adaptive RBF neural network is

$$\hat{f}(\cdot) = \hat{w}^T h(x) \tag{16}$$

where $h(x) = [h_1, \dots, h_5]^T$. \hat{w} is the adaptive weight, and the adaptive law is described as

$$\dot{\hat{w}} = \psi h z^T P B \tag{17}$$

where $\psi > 0$ is the constant gain. B represents the input matrix of the closed-loop system. P is the positive definite matrix, and there exists the matrix $Q \geq 0$ such that P satisfies the stability equation $PA + A^T P = -Q$, where A is the state matrix of the closed-loop system and the equations are given in Section 3.3. The adaptive neural network proposed in this paper recalculates the adaptive weights through the position error, velocity error of the manipulator and the output of the hidden layer of the adaptive neural network in each iteration to achieve the training of the neural network.

Property 2. Given a continuous function $f(\cdot)$, there is an ideal weight \hat{w}^* , and the adaptive neural network approximation error $\gamma = f(\cdot) - \hat{f}^*(\cdot)$ satisfies $\max\|\gamma\| \leq \gamma_0$. γ_0 is the upper bound of error, and satisfies $\gamma_0 \leq \varepsilon$, ε is a very small positive number.

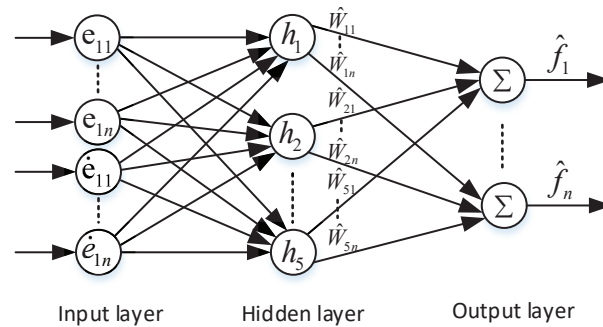


Figure 1. The structure of the Adaptive RBF Neural Network.

3.2. Design of Smooth-Switching for Backstepping Gain

The change in the control gain can produce the contradiction between the system dynamics characteristics and the steady-state characteristics. The larger the gain, the faster the response, the higher the accuracy, but the worse the stability [37,38]. The smaller the gain, the better the stability, but the response time will be longer and the accuracy will be lower. In addition, considering safety in engineering, the control gain is often within a certain range. In this part, a new smooth-switching for backstepping gain strategy is proposed, and the control gain is designed with the error surface and the change rate of the error surface, respectively.

3.2.1. The Variable Control Gain of the Error

Define the error surface as e_{ij} , where the subscript represents the j th component of the i th error surface. The variable control gain designed with error is expressed as

$$\Delta k_{ij}(e_{ij}) = \frac{2\alpha_{ij}}{\pi} \arctan \left(\frac{e_{ij}}{\beta_{ij}} \right)^2 + \delta_{ij} \tag{18}$$

where $\alpha_{ij} > 0$ is the magnification of the gain designed with the error. $\beta_{ij} > 0$ is the scale parameter of variable gain. δ_{ij} is a positive constant, ensure that $\Delta k_{ij}(e_{ij}) > 0, \forall e_{ij} \in R$.

3.2.2. The Variable Control Gain of the Change Rate of the Error

Take the derivative of the error surface e_{ij} to get \dot{e}_{ij} . The variable control gain designed with the change rate of error can be described as

$$\Delta k_{ij}(\dot{e}_{ij}) = \delta_{ij} - \frac{2\xi_{ij}}{\pi} \arctan \left(\frac{\dot{e}_{ij}}{\zeta_{ij}} \right)^2 \tag{19}$$

where $\zeta_{ij} > 0$ is the magnification of the gain function designed based on the change rate of error. ζ_{ij} is the positive scale parameter. $\delta_{ij} > \zeta_{ij}$, ensure that $\Delta k_{ij}(\dot{e}_{ij}) > 0, \forall \dot{e}_{ij} \in R$.

3.2.3. Design of Smooth-Switching for Backstepping Gain

To solve the smoothness of the gain switching transition process, a smooth-switching function based on the error surface is designed as

$$f(e_{ij}) = 1 - \exp\left(-\left(\frac{e_{ij}}{\sigma_{ij}}\right)^2\right) \tag{20}$$

where σ_{ij} is the positive scale constant. The smooth-switching function curve with different values of σ_{ij} are shown in Figure 2.

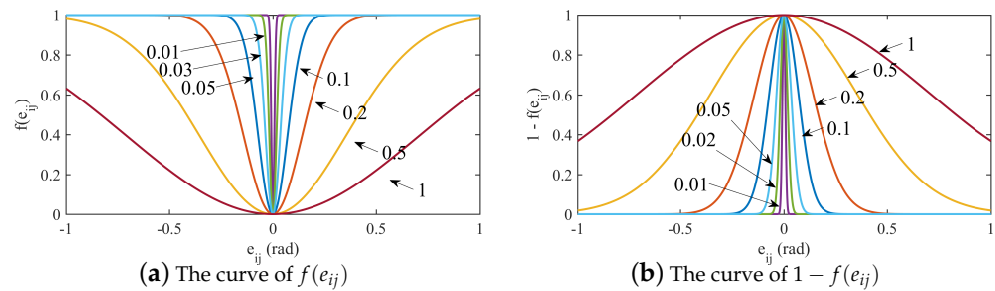


Figure 2. The smooth-switching function curve.

According to (18)–(20), the smooth-switching for backstepping gain strategy is designed as

$$\Delta k_{ij} = f(e_{ij}) \cdot \Delta k_{ij}(e_{ij}) + [1 - f(e_{ij})] \cdot \Delta k_{ij}(\dot{e}_{ij}) \tag{21}$$

When the error is large, the control gain designed based on the error is mainly used. The greater the error, the greater the control gain, which ensures the rapid convergence of the system. When the error is small, the control gain designed by using the change rate of error is mainly used. The larger the change rate of error surface, the smaller the control gain. Thus, the jitter phenomenon caused by the large control gain of the manipulator system in the steady-state is reduced. When the error is in the middle range, the two gain functions transition in the form of smooth switching.

3.3. Design of BLF-ANBG Controller

To consider the time-varying asymmetric output limitation, the time-varying asymmetric BLF and adaptive neural network are used to design the smooth-switching for the backstepping gain controller. The block diagram of the manipulator system based on the BLF-ANBG controller is shown in Figure 3, and the design process is as follows

Step (1) Define the first tracking error surface vector as $e_1 = x_1 - x_d = [e_{11}, \dots, e_{1n}]^T$, x_d is the desired tracking position. The time-varying barrier of output is defined as

$$y_{ai}(t) = x_{di}(t) - y_{i \min}(t) \tag{22}$$

$$y_{bi}(t) = y_{i \max}(t) - x_{di}(t) \tag{23}$$

where $i = 1, \dots, n$, which means the i th component of the vector. Define the time-varying asymmetric output constraints BLF as

$$V_1 = \sum_{i=1}^n V_{1i} = \sum_{i=1}^n \left[\frac{\lambda(e_{1i})}{2} \log \frac{1}{1 - \zeta_{i+}^2(t)} + \frac{1 - \lambda(e_{1i})}{2} \log \frac{1}{1 - \zeta_{i-}^2(t)} \right] \tag{24}$$

where

$$\lambda(e_{1i}) = \begin{cases} 1, & \text{if } e_{1i} > 0 \\ 0, & \text{if } e_{1i} \leq 0 \end{cases} \quad (25)$$

$$\zeta_i \min(t) = \frac{e_{1i}}{y_{ai}(t)}, \zeta_i \max(t) = \frac{e_{1i}}{y_{bi}(t)} \quad (26)$$

Define the coordinate transformation as

$$\zeta_i(t) = (1 - \lambda(e_{1i}))\zeta_i \min(t) + \lambda(e_{1i})\zeta_i \max(t) \quad (27)$$

Substituting (25) and (27) into (24), can obtain

$$V_1 = \sum_{i=1}^n V_{1i} = \sum_{i=1}^n \frac{1}{2} \log \frac{1}{1-\zeta_i^2(t)}, |\zeta_i(t)| \leq 1 \quad (28)$$

It can be obtained from (28) that when $|\zeta_i| \leq 1$, V_1 is positive definite. The differential of V_1 as

$$\begin{aligned} \dot{V}_1 = \sum_{i=1}^n \dot{V}_{1i} = \sum_{i=1}^n & \left[\frac{\lambda(e_{1i})\zeta_i \max(t)}{y_{bi}(t)(1-\zeta_i^2 \max(t))} (e_{2i} + x_{2di} - \dot{x}_{di} - e_{1i} \frac{\dot{y}_{bi}(t)}{y_{bi}(t)}) \right. \\ & \left. + \frac{(1-\lambda(e_{1i}))\zeta_i \min(t)}{y_{ai}(t)(1-\zeta_i^2 \min(t))} (e_{2i} + x_{2di} - \dot{x}_{di} - e_{1i} \frac{\dot{y}_{ai}(t)}{y_{ai}(t)}) \right] \end{aligned} \quad (29)$$

where x_{2di} is the i th component of the virtual control vector x_{2d} , and the virtual control vector x_{2d} is designed by using the backstepping method as

$$x_{2d} = -(\Delta k_1 + \bar{k}_1(t))e_1 + \dot{x}_d \quad (30)$$

$$\Delta k_i = \text{diag}\{\Delta k_{i1}, \dots, \Delta k_{in}\} \quad (31)$$

$$\bar{k}_1(t) = \text{diag}\{\bar{k}_{11}(t), \dots, \bar{k}_{1n}(t)\} \quad (32)$$

where $\bar{k}_{1i}(t) = \sqrt{\left(\frac{\dot{y}_{ai}(t)}{y_{ai}(t)}\right)^2 + \left(\frac{\dot{y}_{bi}(t)}{y_{bi}(t)}\right)^2} + a$, $a > 0$ is a constant to ensure that the derivative of x_{2di} is bounded. Substituting (26) and (27) and (30)–(32) into (29) can be rewritten as

$$\dot{V}_1 = \sum_{i=1}^n \dot{V}_{1i} \leq \sum_{i=1}^n \left[-\frac{\Delta k_{1i}\zeta_i^2}{1-\zeta_i^2} + \left(\frac{1-\lambda(e_{1i})}{y_{ai}^2(t)-e_{1i}^2} + \frac{\lambda(e_{1i})}{y_{bi}^2(t)-e_{1i}^2} \right) e_{1i}e_{2i} \right] \quad (33)$$

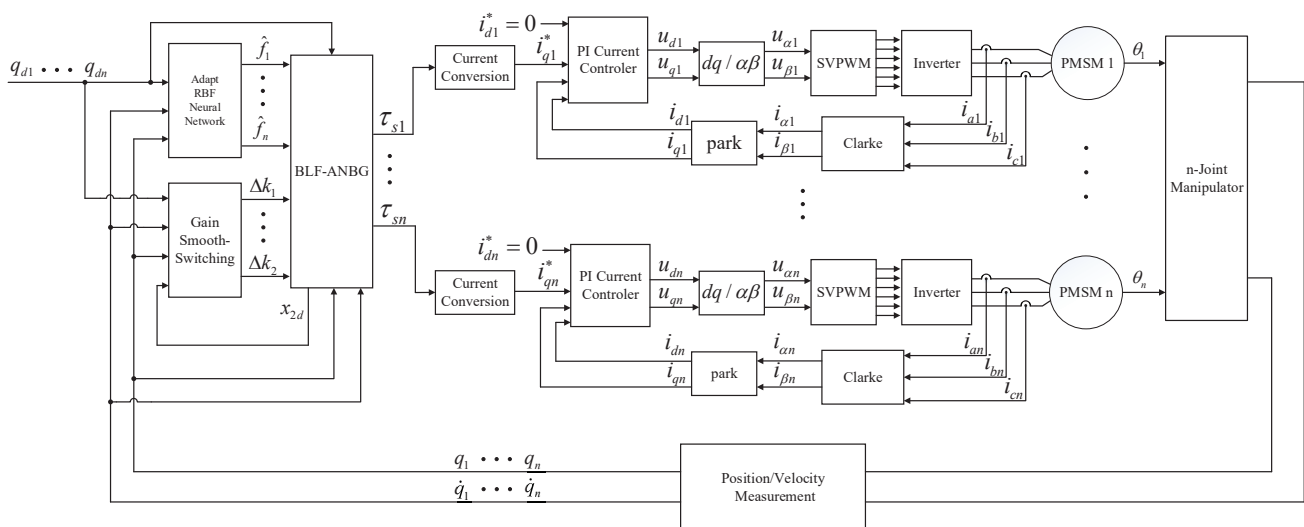


Figure 3. The Block Diagram of the Manipulator System Based on the BLF-ANBG Controller.

Step (2) The second error surface vector is defined as $e_2 = x_2 - x_{2d} = [e_{21}, \dots, e_{2n}]^T$. Define the stability function as $V_2 = \sum_{i=1}^n V_{2i} = \sum_{i=1}^n \frac{1}{2} e_{2i}^2$. Substituting into (13), based on the backstepping control method, the actual control signal is selected as

$$\tau_s = \bar{M}(x_1)[- \Delta k_2 e_2 + \dot{x}_{2d} - \eta e_1] + \bar{C}(x_1, x_2)x_2 + \bar{G}(x_1) + \mu \tau_f - \hat{f} \tag{34}$$

where $\eta = \text{diag} \left\{ \left(\frac{1-\lambda(e_{11})}{y_{a1}^2(t)-e_{11}^2} + \frac{\lambda(e_{11})}{y_{b1}^2(t)-e_{11}^2} \right), \dots, \left(\frac{1-\lambda(e_{1n})}{y_{an}^2(t)-e_{1n}^2} + \frac{\lambda(e_{1n})}{y_{bn}^2(t)-e_{1n}^2} \right) \right\}$, and \hat{f} is the adaptive RBF neural network estimate of f . Substituting (30), Equation (34) can be rewritten as

$$\begin{aligned} \tau_s = \bar{M}(x_1) [\dot{x}_d - (\Delta k_1 + \Delta k_2 + \bar{k}_1(t))\dot{e}_1 - [\Delta k_2(\Delta k_1 + \bar{k}_1(t)) + \eta]e_1] \\ + \bar{C}(x_1, x_2)x_2 + \bar{G}(x_1) + \mu \tau_f - \hat{f} \end{aligned} \tag{35}$$

Substitute (35) into (11), subtracting $\bar{M}(x_1)\dot{x}_2 + \bar{C}(x_1, x_2)x_2 + \bar{G}(x_1)$ from both sides, can get

$$\begin{aligned} \ddot{e}_1 + (\Delta k_1 + \Delta k_2 + \bar{k}_1(t))\dot{e}_1 + [\Delta k_2(\Delta k_1 + \bar{k}_1(t)) + \eta]e_1 = \bar{M}^{-1}(x_1)(f - \hat{f}) \\ = \bar{M}^{-1}(x_1)(f - \hat{f}^* + \hat{f}^* - \hat{f}) = \bar{M}^{-1}(x_1)(\gamma - \tilde{w}^T h) \end{aligned} \tag{36}$$

where $\tilde{w} = \hat{w} - \hat{w}^*$. Let $z = [e_1, \dot{e}_1]^T$, the closed-loop system equation is

$$\dot{z} = Az + B[\bar{M}^{-1}(\gamma - \tilde{w}^T h)] \tag{37}$$

where $A = \begin{bmatrix} 0_n & I_n \\ -\Delta k_2(\Delta k_1 + \bar{k}_1(t)) - \eta & -\Delta k_1 - \Delta k_2 - \bar{k}_1(t) \end{bmatrix}$, $B = \begin{bmatrix} 0 \\ I_n \end{bmatrix}$. 0_n and I_n represent n dimensional zero matrix and identity matrix, respectively.

4. The Analysis of BLF-ANBG Controller

In this section, the stability of the BLF-ANBG strategy is proved. Then, the manipulator joint output constraints are verified as not violated. Finally, the tracking error convergence is proved.

4.1. Proof of BLF-ANBG Controller Stability

The Lyapunov function of the BLF- ANBG controller is defined as

$$\begin{aligned} V = V_1 + V_2 + \frac{1}{2} z^T P z + \frac{1}{2\psi} \|\tilde{w}\|^2 = \sum_{i=1}^n \left[\frac{\lambda(e_{1i})}{2} \log \frac{1}{1-\zeta_{i+}^2(t)} \right. \\ \left. + \frac{1-\lambda(e_{1i})}{2} \log \frac{1}{1-\zeta_{i-}^2(t)} \right] + \sum_{i=1}^n \frac{1}{2} e_{2i}^2 + \frac{1}{2} z^T P z + \frac{1}{2\psi} \|\tilde{w}\|^2 \end{aligned} \tag{38}$$

where $\|\tilde{w}\| = \text{tr}(\tilde{w}^T \tilde{w})$ is the Frobenius norm of \tilde{w} , and also represents the trace of matrix $\tilde{w}^T \tilde{w}$. From (38), it can be known that V is positive definite. Taking the derivative of \tilde{w} and substituting (17) into $\dot{\tilde{w}}$ can obtain

$$\dot{\tilde{w}} = \dot{\hat{w}} - \dot{\hat{w}}^* = \psi h z^T P B \tag{39}$$

Taking the derivative of (38) can be known that

$$\begin{aligned}
 \dot{V} &\leq \sum_{i=1}^n \left[-\frac{\Delta k_{1i} \zeta_i^2}{1-\zeta_i^2} + \left(\frac{1-\lambda(e_{1i})}{y_{ai}^2(t)-e_{1i}^2} + \frac{\lambda(e_{1i})}{y_{bi}^2(t)-e_{1i}^2} \right) e_{1i} e_{2i} \right] \\
 &\quad + \sum_{i=1}^n \left[-\Delta k_{1i} e_{2i}^2 - \left(\frac{1-\lambda(e_{1i})}{y_{ai}^2(t)-e_{1i}^2} + \frac{\lambda(e_{1i})}{y_{bi}^2(t)-e_{1i}^2} \right) e_{1i} e_{2i} \right] \\
 &\quad + \frac{1}{2} [z^T P \dot{z} + \dot{z}^T P z] + \text{tr}(B^T P z h^T \tilde{w}) \\
 &= \sum_{i=1}^n \left[-\frac{\Delta k_{1i} \zeta_i^2}{1-\zeta_i^2} - \Delta k_{1i} e_{2i}^2 \right] + \frac{1}{2} [z^T P \dot{z} + \dot{z}^T P z] + \text{tr}(B^T P z h^T \tilde{w}) \tag{40}
 \end{aligned}$$

Substituting (37) into (40), it becomes

$$\begin{aligned}
 \dot{V} &\leq \sum_{i=1}^n \left[-\frac{\Delta k_{1i} \zeta_i^2}{1-\zeta_i^2} - \Delta k_{1i} e_{2i}^2 \right] + \frac{1}{2} [z^T P A z + z^T P B \gamma - z^T P B \tilde{w}^T h \\
 &\quad + z^T A^T P z + \gamma^T B^T P z - h^T \tilde{w} B^T P z] + \text{tr}(B^T P z h^T \tilde{w}) \tag{41}
 \end{aligned}$$

Noting that $h^T \tilde{w} B^T P z = z^T P B \tilde{w}^T h = \text{tr}(B^T P z h^T \tilde{w})$ and $\gamma^T B^T P z = z^T P B \gamma$, (41) is rewritten as

$$\dot{V} \leq \sum_{i=1}^n \left[-\frac{\Delta k_{1i} \zeta_i^2}{1-\zeta_i^2} - \Delta k_{1i} e_{2i}^2 \right] - \frac{1}{2} z^T Q z + \gamma^T B^T P z \tag{42}$$

Combining **Property 2** to get

$$\dot{V} \leq \sum_{i=1}^n \left[-\frac{\Delta k_{1i} \zeta_i^2}{1-\zeta_i^2} - \Delta k_{1i} e_{2i}^2 \right] - \|z\| \left[\frac{1}{2} \lambda_{\min}(Q) \|z\| - \|\gamma_0\| \lambda_{\max}(P) \right] \tag{43}$$

where $\lambda_{\min}(\cdot)$ and $\lambda_{\max}(\cdot)$ represent the upper and lower bounds of the eigenvalues, respectively. From (43), it can be seen that all signals in the system are uniformly ultimately bounded (UUB) [44,45]. The system is semi-global and practically stable [46].

Remark 1. To satisfy $\dot{V} \leq 0$, choose appropriate controller parameters such that $\|z\| \geq \frac{2\|\gamma_0\| \lambda_{\max}(P)}{\lambda_{\min}(Q)}$. In this paper, the appropriate eigenvalues of Q are selected to satisfy the above conditions to make the system asymptotically converge to the small neighborhood of the origin. When the approximation error γ tends to 0, the system asymptotically converges to the origin.

4.2. Proof That the Manipulator Joint Outputs Constraints Are Not Violated

From (27), it can be obtained that when $e_{1i} < 0$, which yields $\zeta_i(t) = \zeta_{i \min}(t)$, and because $|\zeta_i| \leq 1$ and $y_{ai}(t) > 0$, according to (26) can be known that $-1 < \zeta_{i \min}(t) \leq 0$, then $-y_{ai}(t) < e_{1i}(t) \leq 0$. Similarly, when $e_{1i} \geq 0$, $0 \leq e_{1i}(t) < y_{bi}(t)$ can be obtained. In conclusion, that

$$-y_{ai}(t) < e_{1i}(t) < y_{bi}(t), |\zeta_i(t)| < 1 \tag{44}$$

Adding $x_{di}(t)$ to each term in the inequality, (45) can be rewritten as

$$-y_{ai}(t) + x_{di}(t) < e_{1i}(t) + x_{di}(t) < y_{bi}(t) + x_{di}(t), |\zeta_i(t)| < 1 \tag{45}$$

So $y_{i \min}(t) < y(t) < y_{i \max}(t)$, each joint is within the given constraints.

4.3. Proof of Tracking Error Convergence

According to **Lemma 1** and (38), $V(t) \leq V(0)e^{-\rho t}$, $t \geq 0$ can be obtained [34,47], where $\rho = \min\{2\Delta k_{1j}, 2\Delta k_{2j}\}$, $j = 1, \dots, n$. It can be obtained that

$$\frac{1}{2} \log \frac{1}{1-\zeta_i^2(t)} \leq V(0)e^{-\rho t} \tag{46}$$

Hence,

$$\zeta_i^2(t) \leq 1 - e^{-2V(0)e^{-\rho t}} \tag{47}$$

When $e_{1i} \leq 0$, $\zeta_i(t) = \zeta_i \min(t) = \frac{e_{1i}}{y_{ai}(t)}, -y_{ai}(t) \sqrt{1 - e^{-2V(0)e^{-\rho t}}} \leq e_{1i} \leq 0$. When $e_{1i} > 0$, $\zeta_i(t) = \zeta_i \max(t) = \frac{e_{1i}}{y_{bi}(t)}, 0 < e_{1i} \leq y_{bi}(t) \sqrt{1 - e^{-2V(0)e^{-\rho t}}}$. Combining both cases, can conclude that

$$-y_{ai}(t) \sqrt{1 - e^{-2V(0)e^{-\rho t}}} \leq e_{1i} \leq y_{bi}(t) \sqrt{1 - e^{-2V(0)e^{-\rho t}}} \tag{48}$$

where

$$\lim_{t \rightarrow \infty} \left(-y_{ai}(t) \sqrt{1 - e^{-2V(0)e^{-\rho t}}} \right) = 0 \tag{49}$$

$$\lim_{t \rightarrow \infty} \left(y_{bi}(t) \sqrt{1 - e^{-2V(0)e^{-\rho t}}} \right) = 0 \tag{50}$$

From (49) and (50), the upper and lower bounds of e_{1i} converge to 0, so e_{1i} converges to 0.

5. Simulink Results and Analysis

In this section, the BLF-ANBG control strategy is applied to a 2-DOF manipulator for simulation experiments to verify the feasibility of the strategy. The simulation experiment is divided into three parts. First, to verify the effectiveness of the smooth-switching for the backstepping control method, it is compared with the two variable gains functions without the smooth-switching strategy. Second, the BLF-ANBG strategy is used to control the manipulator to track the unit-step and periodic signals without modeling error and unknown load, and compare with other commonly used control strategies. Finally, the BLF-ANBG strategy is compared with the commonly used strategies in the presence of modeling errors and unknown loads. The parameters of the manipulator system in all simulation experiments in this section are shown in Table 1.

Table 1. The parameters of the manipulator system.

Parameters	Values	Parameters	Values
Weight (m_1, m_2)	0.5 kg	Length (l_1, l_2)	1 m
R_f	$diag\{5, 5\}$ N	R_s	$diag\{2.875, 2.875\}$ Ω
n_p	$diag\{4, 4\}$	L_d, L_q	$diag\{0.0085, 0.0085\}$ H
Φ	$diag\{0.175, 0.175\}$ Wb	J_m	$diag\{0.0025, 0.0025\}$ kg · m ²
η	$diag\{0.01, 0.01\}$	R_m	$diag\{6, 6\}$ N
F_c	$diag\{3, 3\}$ N	Sampling Period	0.0001 s

The dynamics model of the 2-DOF manipulator system can be described as (8), where the inertia matrix $M(q)$, Coriolis force matrix $C(q, \dot{q})$ and gravity matrix $G(q)$ can be defined as

$$M(q) = \begin{bmatrix} M_{11} & M_{12} \\ M_{21} & M_{22} \end{bmatrix}, C(q, \dot{q}) = \begin{bmatrix} C_{11} & C_{12} \\ C_{21} & C_{22} \end{bmatrix}, G(q) = \begin{bmatrix} G_1 \\ G_2 \end{bmatrix}$$

where

$$\left\{ \begin{array}{l} M_{11} = m_1 l_1^2 + m_2 l_1^2 + m_2 l_2^2 + 2m_2 l_1 l_2 \cos q_2 \\ M_{12} = M_{21} = m_2 l_2^2 + m_2 l_1 l_2 \cos q_2 \\ M_{22} = m_2 l_2^2 \\ C_{11} = -m_2 l_1 l_2 \dot{q}_2 \sin q_2 \\ C_{12} = -m_2 l_1 l_2 \dot{q}_1 \sin q_2 - m_2 l_1 l_2 \dot{q}_2 \sin q_2 \\ C_{21} = m_2 l_1 l_2 \dot{q}_1 \sin q_2 \\ C_{22} = 0 \\ G_1 = m_1 l_1 g \cos q_1 + m_2 l_1 g \cos q_1 + m_2 l_2 g \cos(q_1 + q_2) \\ G_2 = m_2 l_2 g \cos(q_1 + q_2) \end{array} \right. \quad (51)$$

The parameters of the BLF-ANBG controller are described in Table 2.

Table 2. The parameters of controller.

Parameters	Values	Parameters	Values	Parameters	Values
β_{11}, β_{12}	0.5	ζ_{11}, ζ_{12}	0.5	β_{21}, β_{22}	0.05
ζ_{21}, ζ_{22}	0.05	σ_{11}, σ_{12}	0.5	σ_{21}, σ_{22}	10
δ_{11}, δ_{12}	2000	δ_{21}, δ_{22}	270	α_{11}, α_{12}	1000
α_{21}, α_{22}	5	ξ_{11}, ξ_{12}	1800	ξ_{21}, ξ_{22}	250
ε	0.1	ψ	10	Q	$diag\{60, 60, 60, 60\}$

From Table 2, $0 < \beta_{ij} < 1, 0 < \zeta_{ij} < 1$, the values of β_{ij} and ζ_{ij} are obtained by trial and error within an appropriate range. When β_{ij} and ζ_{ij} are larger, the dynamic response of the system is faster, and when β_{ij} and ζ_{ij} are smaller, the transition process is smoother. If α_{ij} is larger, the upper bound of the variable gain function of the error is larger, and the systems response is faster, which can be appropriately increased on the premise of ensuring the safety of the system. δ_{ij} is the lower and upper bounds of the two gain functions, and $\delta_{ij} > \xi_{ij}$ ensures that the system is stable. Q can be appropriately increased to enhance the system convergence effect.

5.1. Simulation Comparison Results of Smooth-Switching for Backstepping Gain Strategy

In this part, the manipulator system uses the smooth-switching for backstepping gain strategy to track the unit-step signal, and compares it with two variable gain functions without the smooth-switching strategy. The initial position of each joint of the manipulator system is $q(0) = [0, 0]^T$, the execution saturation is ± 20 N·m, and the output constraints of each joint are $y_{i \min} = -0.3 + 0.1 \sin(0.8t + \frac{\pi}{3}), y_{i \max} = 1.3 + 0.2 \sin(0.5t + \frac{\pi}{2})$. The tracking and error curves for the unit-step signal are provided in Figure 4.

As can be seen from Figure 4, using only the gain function based on the error has a faster response speed and can reach the steady-state faster, but there will be overshoot, and large jitter will occur after reaching the steady state. Using only the gain function based on the change rate of error can improve steady-state performance but has a long response time. The smooth-switching for backstepping gain strategy combines the advantages of two gain functions and can have good dynamic and steady-state performances at the same time.

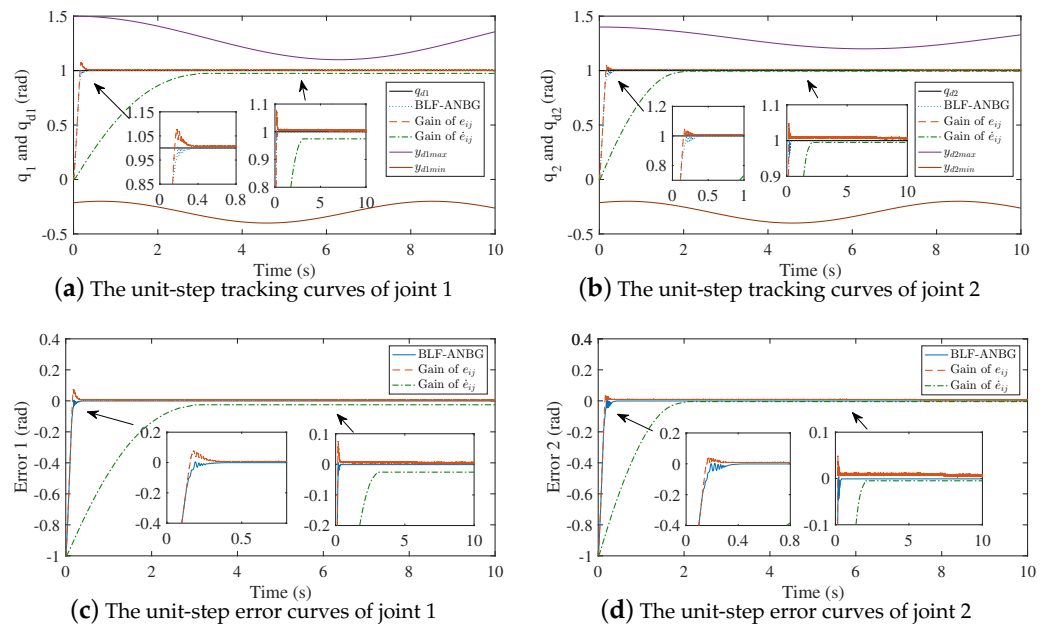


Figure 4. The unit-step tracking curves compared to two variable gain functions.

5.2. Without Modeling Error and Unknown Load

In this part, the manipulator tracks the unit-step signal and the expected periodic signal $q_d = [0.8\sin(0.5t + \frac{\pi}{2}), 0.9\sin(0.8t + \frac{\pi}{3})]^T$ without modeling error and load, respectively. The input torque saturation of each joint is ± 20 N-m. The joint constraints that track the unit-step signal are $y_{i\min} = -0.3 + 0.1\sin(0.8t + \frac{\pi}{3})$, $y_{i\max} = 1.3 + 0.2\sin(0.5t + \frac{\pi}{2})$. The joint constraints that track the periodic signal signal are $y_{i\min} = -1.1 + 0.1\sin(0.6t + \frac{\pi}{3})$, $y_{i\max} = 1.2 + 0.2\sin(0.5t)$. The proposed BLF-ANBG strategy is compared with the conventional backstepping strategy under large gain and small gain. The tracking and error curves for the unit-step signal and periodic signal are as shown in Figures 5 and 6. The dynamic performance and steady-state performance of the tracking two signals are as shown in Table 3.

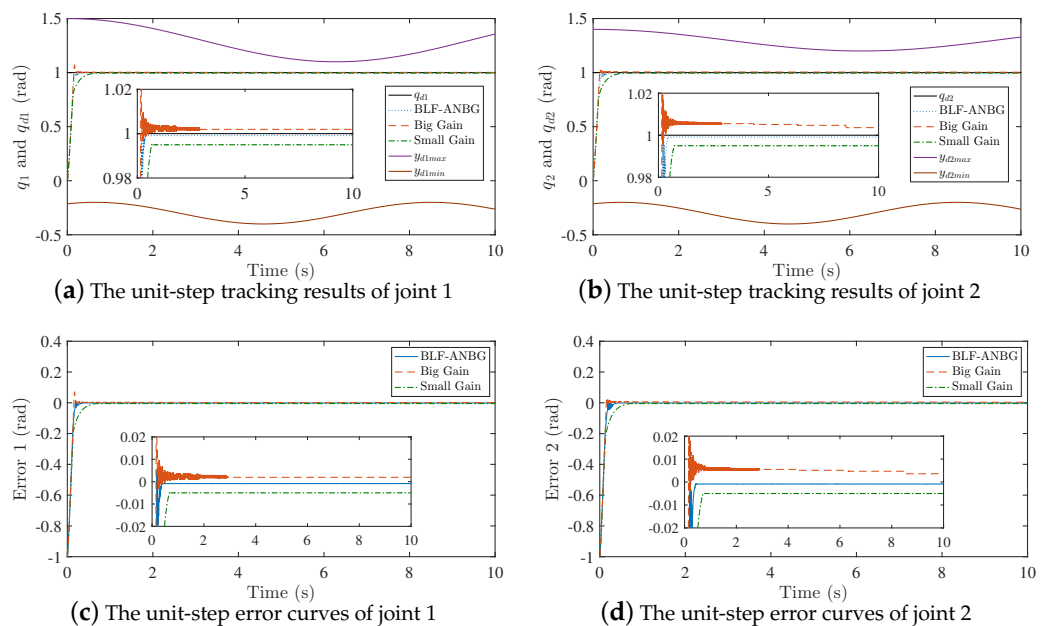


Figure 5. The unit-step tracking curves compared to traditional backstepping.

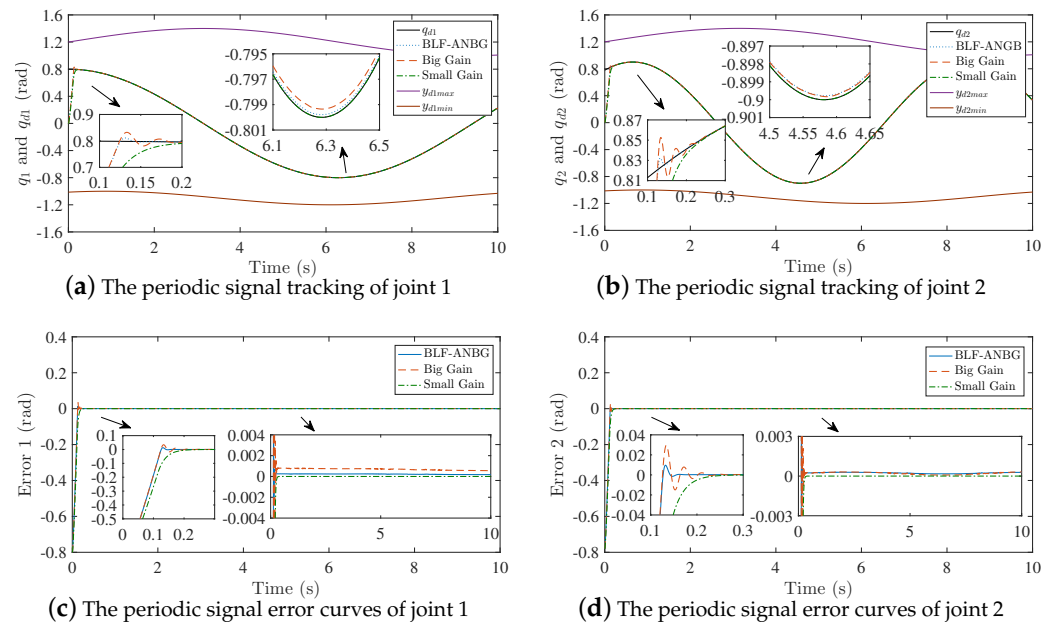


Figure 6. The periodic signal tracking curves compared to traditional backstepping.

Table 3. The rise time and error range compared to traditional backstepping.

Signal	Joint	Description	BLF-ANBG	Big Gain	Small Gain
Unit-step	joint 1	Rise Times (s)	0.1865	0.1525	0.6653
		Tracking Error (rad)	± 0.0013	± 0.0095	± 0.0059
		Jitter Range (rad)	0.0005	0.032	0.0002
	joint 2	Rise Times (s)	0.1894	0.1503	0.6712
		Tracking Error (rad)	± 0.0011	± 0.0065	± 0.0004
		Jitter Range (rad)	0.00054	0.0035	0.0001
Period	joint 1	Rise Times (s)	0.1255	0.1244	0.2312
		Tracking Error (rad)	± 0.0013	± 0.0342	± 0.0011
		Jitter Range (rad)	0.0007	0.0022	0.0001
	joint 2	Rise Times (s)	0.1269	0.1255	0.2716
		Tracking Error (rad)	± 0.0009	± 0.0296	± 0.0005
		Jitter Range (rad)	0.00011	0.00025	0.00001

From these figures and tables, it is easy to see that the joint outputs are all within the given constraints. The fixed gain of the traditional backstepping strategy without smooth-switching for gain can affect the performance of the system tracking. When the gain is large, although the system reaches the steady state in 0.1525 s and the accuracy is high, the system has a large jitter in the steady state, and the jitter range is 0.032 rad. When the gain is small, the jitter range is 0.0002 rad, which is smaller than that when the gain is large, but the system reaches the steady state at 0.6712 s and the accuracy is low. Therefore, the value of the backstepping gain will cause the contradiction between the dynamic characteristics and the steady-state characteristics of the system. When the BLF- ANBG strategy is applied, this contradiction can be effectively solved, the system can quickly reach the steady state and have better steady-state performance.

Secondly, the feasibility of this strategy is verified by comparing two commonly used SMC strategies and PD gravity compensation strategies. The tracking and error curves of the unit-step signal and periodic signal of the three strategies are presented in Figures 7 and 8, respectively. The tracking performances are shown in Table 4.

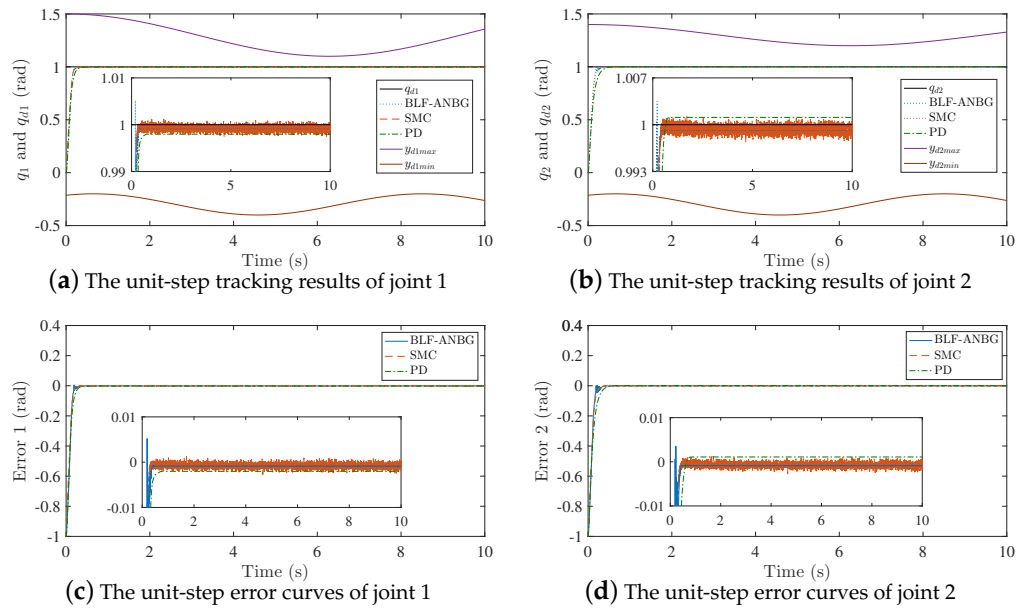


Figure 7. The unit-step signal tracking and error curves of the three strategies.

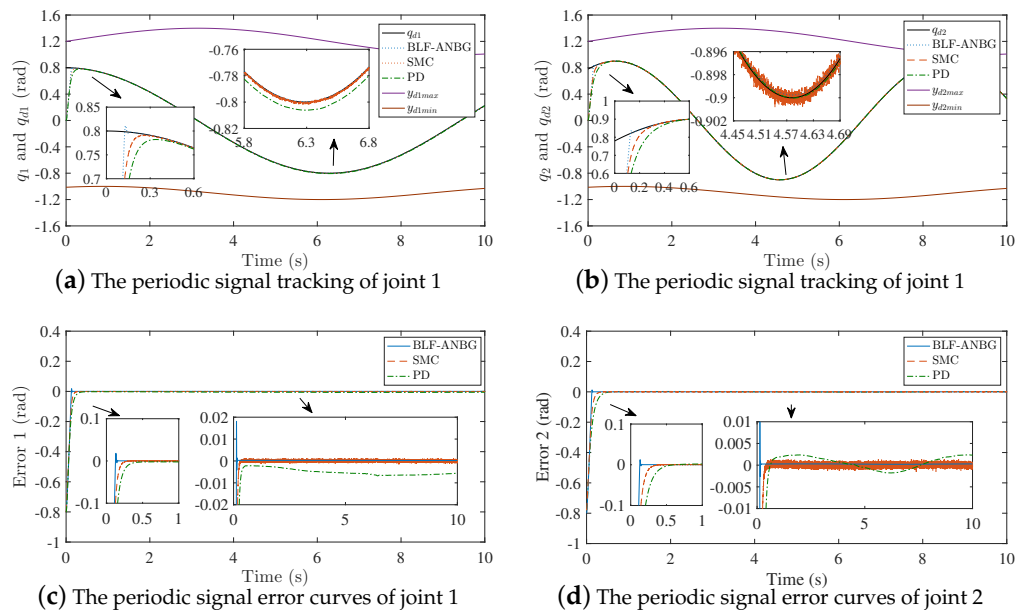


Figure 8. The expected periodic signal tracking and error curves of the three strategies.

Table 4. The rise time and error range without modeling error and load.

Signal	Joint	Description	BLF-ANBG	SMC	PD
Unit-step	joint 1	Rise Times (s)	0.1865	0.267	0.5041
		Tracking Error (rad)	± 0.0013	± 0.002	± 0.0021
	joint 2	Rise Times (s)	0.1894	0.296	0.6201
		Tracking Error (rad)	± 0.0011	± 0.002	± 0.0011
Period	joint 1	Rise Times (s)	0.1255	0.1956	0.3913
		Tracking Error (rad)	± 0.0013	± 0.0023	± 0.0067
	joint 2	Rise Times (s)	0.1269	0.2154	0.4541
		Tracking Error (rad)	± 0.0009	± 0.0021	± 0.0024

It can be seen from Figures 7 and 8 and Table 4 that the SMC can quickly reach the steady-state when tracking the unit-step signal and the periodic signal, but the chattering phenomenon occurs, and the jitter range of each joint is 0.004 rad and 0.0046 rad. The jitter of the PD gravity compensation strategy is obviously reduced, yet the tracking accuracy is poor, and the tracking error is ± 0.0067 rad. Compared with these two strategies, BLF-ANBG has better tracking accuracy and stability, and can reach steady state faster.

5.3. With Modeling Error and Unknown Load

In this part, time-varying modeling errors and time-varying unknown loads are added to simulate the tracking effect of the manipulator in practical engineering applications. The controller parameters are the same as in Table 2. The parameters of modeling error and unknown load are described in Table 5.

Table 5. The parameters of modeling error and unknown load.

Parameters	Values	Parameters	Values
$\Delta M(q)$	$0.15M(q)$	$\Delta C(q, \dot{q})$	$0.25C(q, \dot{q})$
$\Delta G(q)$	$0.2M(q)$	ΔJ_m	$0.1J_m$
τ_L	$\begin{bmatrix} 10 \sin(0.5t + \pi/2) \\ 10 \sin(0.5t + \pi/2) \end{bmatrix}$	ΔE	$\begin{bmatrix} 0.1 \cos 0.5t \\ 0.1 \cos 0.5t \end{bmatrix}$

To verify the performance of the BLF-ANBG strategy, the BLF-GSS strategy, the SMC strategy and the PD gravity compensation strategy are used for comparison. The initial position of the joint is 0. The approximation curves of the adaptive neural network strategy are shown in Figure 9.

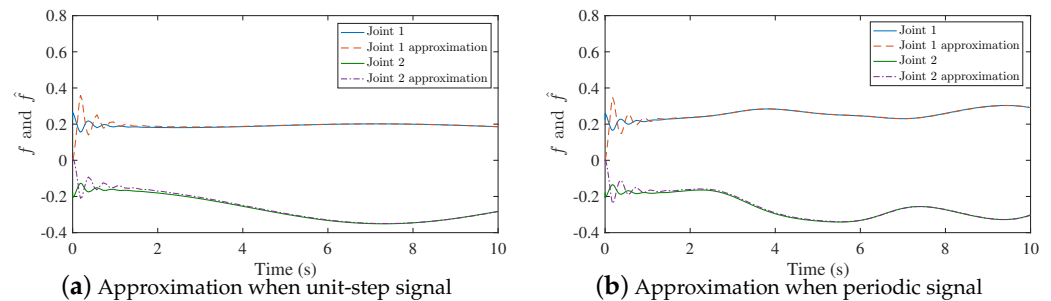


Figure 9. The approximation curves for the unit-step signal and expected periodic signal.

Figure 9 clearly shows that although the adaptive neural network has large approximation error in the initial stage, it can effectively approximate the modeling error and unknown load within 2 s. The tracking result and error curves of the unit-step signal are given in Figure 10, the tracking result and error curves of the expected periodic signal are provided in Figure 11. The controller performance is shown in Table 6.

According to Figures 10 and 11 and Table 6, it can be known that modeling errors and unknown loads have an impact on the tracking accuracy of the manipulator. In the absence of adaptive neural network compensation, the BLF-GSS strategy, the SMC strategy and the PD gravity compensation strategy all generate large tracking errors; the maximum tracking errors of the three strategies are ± 0.0007 rad, ± 0.0022 rad, ± 0.0054 rad. The BLF-ANBG strategy can effectively reduce the modeling error and the influence of unknown loads, and can cause each joint to reach the steady-state within 0.156 s; the steady-state accuracy is also high. At the same time, the joints are all within the given constraints.

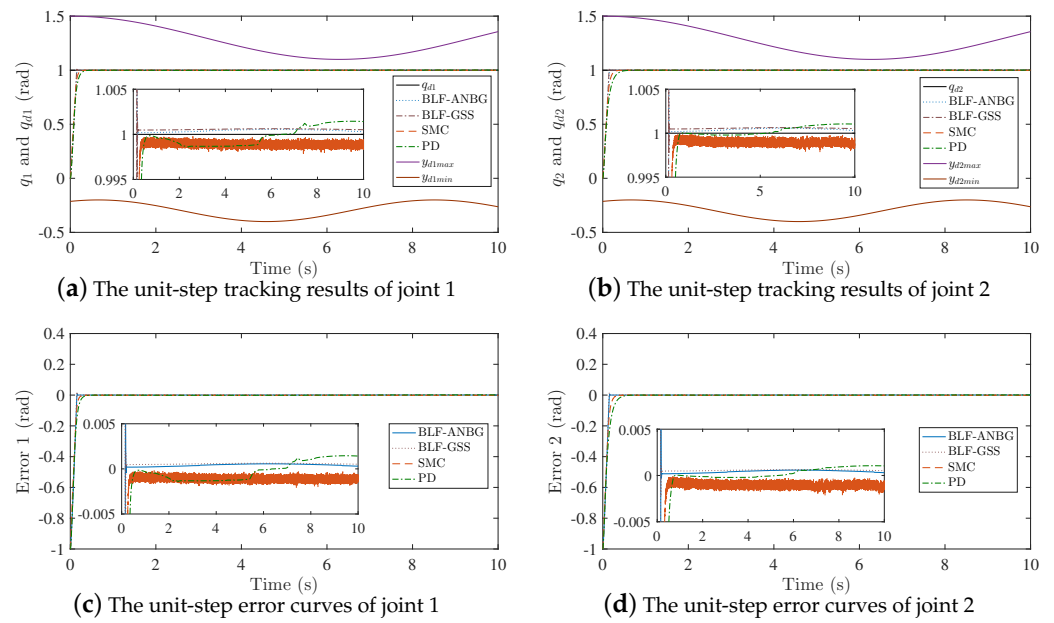


Figure 10. The unit-step signal tracking and error curves of the four strategies.

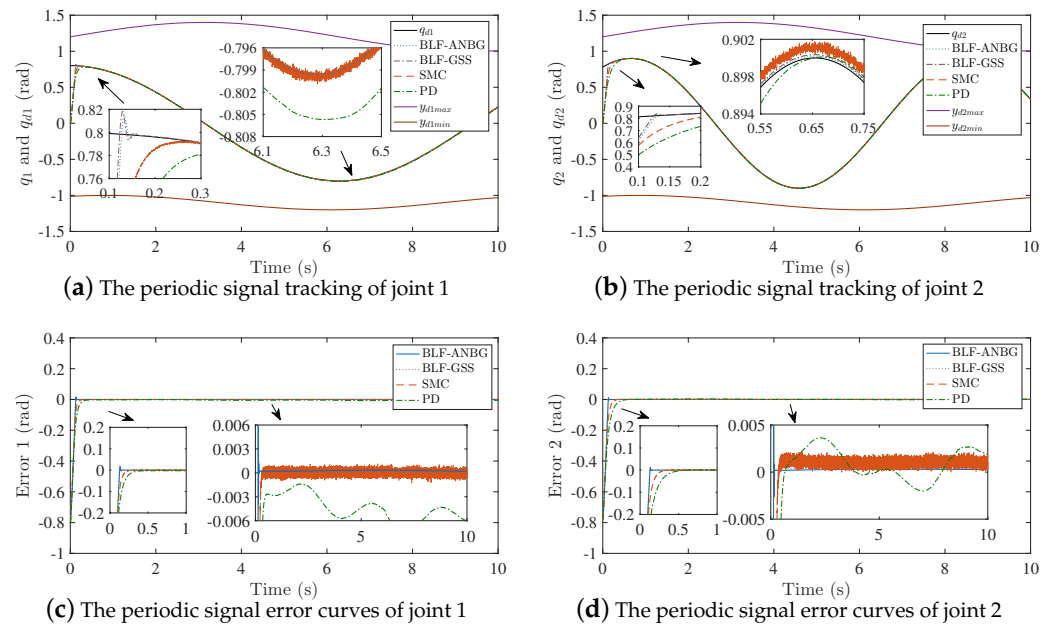


Figure 11. The expected periodic signal tracking and error curves of the four strategies.

Table 6. The tracking performance with modeling error and load.

Signal	Joint	Description	BLF-ANBG	BLF-GSS	SMC	PD
Unit-step	joint 1	Rise Times (s)	0.1562	0.1506	0.2817	0.4634
		Tracking Error (rad)	±0.0005	±0.0006	±0.0016	±0.0014
	joint 2	Rise Times (s)	0.1552	0.1496	0.2142	0.5652
		Tracking Error (rad)	±0.0005	±0.0007	±0.002	±0.0012
Period	joint 1	Rise Times (s)	0.1247	0.1235	0.2721	0.4254
		Tracking Error (rad)	±0.0002	±0.0004	±0.0017	±0.0054
	joint 2	Rise Times (s)	0.1223	0.1269	0.3256	0.4481
		Tracking Error (rad)	±0.0003	±0.0006	±0.0022	±0.0047

Summarizing the above results, the strategy proposed in this article can track the desired position signal quickly and stably in the presence of modeling errors and unknown loads. The contradiction between dynamic and steady-state caused by backstepping method gain is significantly improved.

6. Conclusions

This article presents a new tracking control strategy to solve the contradiction between the dynamic and steady-state characteristic caused by the control gain of the manipulator when there are uncertain interference terms. In this work, an overall model of the manipulator driven by PMSM with multiple constraints, modeling errors, and unknown loads is established. The proposed BLF-ANBG control strategy is applied to the 2-DOF manipulator. The simulation comparison shows that the proposed control strategy can effectively improve the contradiction between the dynamic and the steady-state performances of the system, and make the system take into account both excellent dynamic and steady-state characteristics. Additionally, the strategy effectively compensates for model errors, external disturbances and actuator saturation, while limiting the output of the system within the time-varying asymmetric constraint, which is more suitable for practical engineering needs. In actual engineering, the state of the speed and acceleration of the manipulator will also be constrained. In the future work, we will work hard to solve the problem of the full-state constraints of the manipulator system.

Author Contributions: Conceptualization, H.Y. (Haisheng Yu) and Q.Y.; methodology, Q.Y.; software, Q.Y.; validation, X.M., W.Y. and H.Y. (Huan Yang); formal analysis, Q.Y.; investigation, Q.Y.; resources, H.Y. (Haisheng Yu); data curation, X.M.; writing—original draft preparation, Q.Y.; writing—review and editing, X.M.; visualization, W.Y. and H.Y. (Huan Yang); supervision, H.Y. (Huan Yang); project administration, H.Y. (Haisheng Yu); funding acquisition, H.Y. (Haisheng Yu). All authors have read and agreed to the published version of the manuscript.

Funding: This work was supported by the National Natural Science Foundation of China with grant number 61573203 and the Shandong Province Natural Science Foundation with grant number ZR2021MF005.

Institutional Review Board Statement: Not applicable.

Informed Consent Statement: Not applicable.

Data Availability Statement: Not applicable.

Conflicts of Interest: The authors declare no conflict of interest.

Abbreviations

The following abbreviations are used in this manuscript:

BLF	Barrier Lyapunov Function
ANBG	smooth-switching for backstepping gain based on adaptive neural network
DOF	degree of freedom
PMSM	permanent magnet synchronous motor
PID	proportional integral derivative
SMC	sliding mode control
GSS	smooth-switching for backstepping gain
UUB	uniformly ultimately bounded

References

1. Saab, S.S.; Ghanem, P. A Multivariable Stochastic Tracking Controller for Robot Manipulators without Joint Velocities. *IEEE Trans. Autom. Control* **2018**, *63*, 2481–2495. [[CrossRef](#)]
2. Nguyen, V.C.; Le, P.N.; Kang, H.J. An Active Fault-Tolerant Control for Robotic Manipulators Using Adaptive Non-Singular Fast Terminal Sliding Mode Control and Disturbance Observer. *Actuators* **2021**, *10*, 332. [[CrossRef](#)]
3. Park, K.M.; Kim, J.; Park, J.; Park, F.C. Learning-Based Real-Time Detection of Robot Collisions without Joint Torque Sensors. *IEEE Robot. Autom. Lett.* **2021**, *6*, 103–110. [[CrossRef](#)]

4. Li, L.; Xiao, J.; Zhao, Y.; Liu, K.; Li, K. Robust position anti-interference control for PMSM servo system with uncertain disturbance. *CES Trans. Electrical Mach. Syst.* **2020**, *4*, 10. [[CrossRef](#)]
5. Yu, Y.; Cong, L.; Tian, X.; Mi, Z.; Li, Y.; Fan, Z.; Fan, H. A stator current vector orientation based multi-objective integrative suppressions of flexible load vibration and torque ripple for PMSM considering electrical loss. *CES Trans. Electrical Mach. Syst.* **2020**, *4*, 161–171. [[CrossRef](#)]
6. Hong, D.K.; Hwang, W.; Lee, J.Y.; Woo, B.C. Design, Analysis, and Experimental Validation of a Permanent Magnet Synchronous Motor for Articulated Robot Applications. *IEEE Trans. Magn.* **2018**, *54*, 1–4. [[CrossRef](#)]
7. Wen, S.; Qin, G.; Zhang, B.; Lam, H.; Zhao, Y.; Wang, H. The study of model predictive control algorithm based on the force/position control scheme of the 5-DOF redundant actuation parallel robot. *Robot. Auton. Syst.* **2016**, *79*, 12–25. [[CrossRef](#)]
8. Pradhan, S.K.; Subudhi, B. Position control of a flexible manipulator using a new nonlinear self-tuning PID controller. *IEEE/CAA J. Autom. Sin.* **2020**, *7*, 136–149. [[CrossRef](#)]
9. Shojaei, K.; Kazemy, A.; Chatraei, A. An Observer-Based Neural Adaptive PID^2 Controller for Robot Manipulators Including Motor Dynamics with a Prescribed Performance. *IEEE/ASME Trans. Mechatron.* **2021**, *26*, 1689–1699. [[CrossRef](#)]
10. Kim, M.J.; Chung, W.K. Disturbance-Observer-Based PD Control of Flexible Joint Robots for Asymptotic Convergence. *IEEE Trans. Robot.* **2015**, *31*, 1508–1516. [[CrossRef](#)]
11. Feng, Y.; Yu, X.; Man, Z. Non-singular terminal sliding mode control of rigid manipulators. *Automatica* **2002**, *38*, 2159–2167. [[CrossRef](#)]
12. Yeh, Y.L. Output Feedback Tracking Sliding Mode Control for Systems with State- and Input-Dependent Disturbances. *Actuators* **2021**, *10*, 117. [[CrossRef](#)]
13. Huang, A.C.; Chen, Y.C. Adaptive sliding control for single-link flexible-joint robot with mismatched uncertainties. *IEEE Trans. Control Syst. Technol.* **2004**, *12*, 770–775. [[CrossRef](#)]
14. Buondonno, G.; De Luca, A. Efficient Computation of Inverse Dynamics and Feedback Linearization for VSA-Based Robots. *IEEE Robot. Autom. Lett.* **2016**, *1*, 908–915. [[CrossRef](#)]
15. Meng, X.; Yu, H.; Zhang, J.; Xu, T.; Wu, H.; Yan, K. Disturbance Observer-Based Feedback Linearization Control for a Quadruple-Tank Liquid Level System. *ISA Trans.* **2021**, *122*, 146–162. [[CrossRef](#)]
16. Bagheri, M.; Karafyllis, I.; Naseradinmousavi, P.; Krstic, M. Adaptive control of a two-link robot using batch least-square identifier. *IEEE/CAA J. Autom. Sin.* **2021**, *8*, 86–93. [[CrossRef](#)]
17. Yoo, B.K.; Ham, W.C. Adaptive control of robot manipulator using fuzzy compensator. *IEEE Trans. Fuzzy Syst.* **2000**, *8*, 186–199.
18. Wang, H. Adaptive Control of Robot Manipulators with Uncertain Kinematics and Dynamics. *IEEE Trans. Autom. Control* **2017**, *62*, 948–954. [[CrossRef](#)]
19. Kanellakopoulos, I.; Kokotovic, P.; Morse, A. Systematic design of adaptive controllers for feedback linearizable systems. *IEEE Trans. Autom. Control* **1991**, *36*, 1241–1253. [[CrossRef](#)]
20. Cheng, X.; Zhang, Y.; Liu, H.; Wollherr, D.; Buss, M. Adaptive neural backstepping control for flexible-joint robot manipulator with bounded torque inputs. *Neurocomputing* **2021**, *458*, 70–86. [[CrossRef](#)]
21. Farrell, J.A.; Polycarpou, M.; Sharma, M.; Dong, W. Command Filtered Backstepping. *IEEE Trans. Autom. Control* **2009**, *54*, 1391–1395. [[CrossRef](#)]
22. Chang, W.; Li, Y.; Tong, S. Adaptive Fuzzy Backstepping Tracking Control for Flexible Robotic Manipulator. *IEEE/CAA J. Autom. Sin.* **2021**, *8*, 1923–1930. [[CrossRef](#)]
23. Yang, C.; Jiang, Y.; Na, J.; Li, Z.; Cheng, L.; Su, C.Y. Finite-Time Convergence Adaptive Fuzzy Control for Dual-Arm Robot with Unknown Kinematics and Dynamics. *IEEE Trans. Fuzzy Syst.* **2019**, *27*, 574–588. [[CrossRef](#)]
24. Ling, S.; Wang, H.; Liu, P.X. Adaptive Fuzzy Tracking Control of Flexible-Joint Robots Based on Command Filtering. *IEEE Trans. Ind. Electron.* **2020**, *67*, 4046–4055. [[CrossRef](#)]
25. Wai, R.J.; Yang, Z.W. Adaptive Fuzzy Neural Network Control Design via a T-S Fuzzy Model for a Robot Manipulator Including Actuator Dynamics. *IEEE Trans. Syst. Man Cybern. Part B* **2008**, *38*, 1326–1346.
26. Liu, Q.; Li, D.; Ge, S.S.; Ji, R.; Ouyang, Z.; Tee, K.P. Adaptive bias RBF neural network control for a robotic manipulator. *Neurocomputing* **2021**, *447*, 213–223. [[CrossRef](#)]
27. Narayanan, V.; Jagannathan, S.; Ramkumar, K. Event-Sampled Output Feedback Control of Robot Manipulators Using Neural Networks. *IEEE Trans. Neural Netw. Learn. Syst.* **2019**, *30*, 1651–1658. [[CrossRef](#)]
28. Zhang, Z.; Li, Z.; Zhang, Y.; Luo, Y.; Li, Y. Neural-Dynamic-Method-Based Dual-Arm CMG Scheme with Time-Varying Constraints Applied to Humanoid Robots. *IEEE Trans. Neural Netw. Learn. Syst.* **2015**, *26*, 3251–3262. [[CrossRef](#)]
29. Singh, A.P.; Deb, D.; Agarwal, H. On selection of improved fractional model and control of different systems with experimental validation. *Commun. Nonlinear Sci. Numer. Simul.* **2019**, *79*, 104902. [[CrossRef](#)]
30. Singh, A.P.; Deb, D.; Agarwal, H.; Bingi, K.; Ozana, S. Modeling and Control of Robotic Manipulators: A Fractional Calculus Point of View. *Arab. J. Sci. Eng.* **2021**, *46*, 9541–9552. [[CrossRef](#)]
31. Singh, A.P.; Deb, D.; Agrawal, H.; Balas, V.E. Fractional Modeling of Robotic Systems. In *Fractional Modeling and Controller Design of Robotic Manipulators: With Hardware Validation*; Springer International Publishing: Berlin/Heidelberg, Germany, 2021; pp. 19–43.
32. Meng, X.; Yu, H.; Zhang, J.; Yan, K. Optimized control strategy based on EPCH and DBMP algorithms for quadruple-tank liquid level system. *J. Process. Control* **2022**, *110*, 121–132. [[CrossRef](#)]

33. Liu, A.; Yu, H. Smooth-Switching Control of Robot-Based Permanent-Magnet Synchronous Motors via Port-Controlled Hamiltonian and Feedback Linearization. *Energies* **2020**, *13*, 5731. [[CrossRef](#)]
34. Tee, K.P.; Ren, B.; Ge, S.S. Control of nonlinear systems with time-varying output constraints. *Automatica* **2011**, *47*, 2511–2516. [[CrossRef](#)]
35. Liu, A.; Li, H. Stabilization of Delayed Boolean Control Networks with State Constraints: A Barrier Lyapunov Function Method. *IEEE Trans. Circ. Syst. II Express Briefs* **2021**, *68*, 2553–2557. [[CrossRef](#)]
36. Fuentes-Aguilar, R.Q.; Chairez, I. Adaptive Tracking Control of State Constraint Systems Based on Differential Neural Networks: A Barrier Lyapunov Function Approach. *IEEE Trans. Neural Netw. Learn. Syst.* **2020**, *31*, 5390–5401. [[CrossRef](#)]
37. Yoo, S.J.; Park, J.B.; Choi, Y.H. Adaptive Output Feedback Control of Flexible-Joint Robots Using Neural Networks: Dynamic Surface Design Approach. *IEEE Trans. Neural Netw.* **2008**, *19*, 1712–1726.
38. Cheng, X.; Liu, H.; Lu, W. Chattering-Suppressed Sliding Mode Control for Flexible-Joint Robot Manipulators. *Actuators* **2021**, *10*, 288. [[CrossRef](#)]
39. Yueneng, Y.; Ye, Y. Backstepping sliding mode control for uncertain strict-feedback nonlinear systems using neural-network-based adaptive gain scheduling. *J. Syst. Eng. Electron.* **2018**, *29*, 580–586.
40. Zhou, Q.; Zhao, S.; Li, H.; Lu, R.; Wu, C. Adaptive Neural Network Tracking Control for Robotic Manipulators with Dead Zone. *IEEE Trans. Neural Netw. Learn. Syst.* **2019**, *30*, 3611–3620. [[CrossRef](#)]
41. Li, B.; Lin, H.; Xing, H. Adaptive adjustment of iterative learning control gain matrix in Harsh noise environment. *J. Syst. Eng. Electron.* **2013**, *24*, 128–134. [[CrossRef](#)]
42. Li, H.; Liu, Q.; Feng, G.; Zhang, X. Leader–follower consensus of nonlinear time-delay multiagent systems: A time-varying gain approach. *Automatica* **2021**, *126*, 109444. [[CrossRef](#)]
43. Fromion, V.; Monaco, S.; Normand-Cyrot, D. Asymptotic properties of incrementally stable systems. *IEEE Trans. Autom. Control* **1996**, *41*, 721–723. [[CrossRef](#)]
44. Feng, G. A compensating scheme for robot tracking based on neural networks. *Robot. Auton. Syst.* **1995**, *15*, 199–206. [[CrossRef](#)]
45. Wang, M.; Huang, L.; Yang, C. NN-Based Adaptive Tracking Control of Discrete-Time Nonlinear Systems with Actuator Saturation and Event-Triggering Protocol. *IEEE Trans. Syst. Man Cybern. Syst.* **2021**, *51*, 7613–7621. [[CrossRef](#)]
46. Yu, Z.; Yang, Y.; Li, S.; Sun, J. Observer-Based Adaptive Finite-Time Quantized Tracking Control of Nonstrict-Feedback Nonlinear Systems With Asymmetric Actuator Saturation. *IEEE Trans. Syst. Man Cybern. Syst.* **2020**, *50*, 4545–4556. [[CrossRef](#)]
47. Li, G.; Yu, J.; Chen, X. Adaptive Fuzzy Neural Network Command Filtered Impedance Control of Constrained Robotic Manipulators with Disturbance Observer. *IEEE Trans. Neural Netw. Learn. Syst.* **2021**, 1–10. [[CrossRef](#)]